

Augmented-plane-wave approach to scattering of Bloch electrons by an interface

E. E. Krasovskii

Institut für Theoretische Physik, Christian-Albrechts-Universität, Leibnizstrasse 15, D-24098 Kiel, Germany

(Received 26 May 2004; published 28 December 2004)

A full-potential augmented-plane-wave-based variational method is proposed to construct the scattering wave function for a system consisting of two semi-infinite crystals separated by an interface region. The two half spaces are represented by their complex band structures, and a basis set expansion is used to represent the wave function in the embedded region. The method is based on solving the equation $\hat{\gamma}(\hat{H}-E)\Psi=0$ in the scattering region, which is equivalent to the original Schrödinger equation, and the presence of the operator $\hat{\gamma}$ makes it possible to formulate the variational problem in terms of plane waves. Current conservation considerations are drawn on to include the requirement of the smooth continuity of the wave function into the variational functional. The problem of the overcompleteness of embedding basis sets is discussed and a solution is presented. The method is verified by calculating the electron diffraction and surface states on (100) and (111) surfaces of Al and Cu. The accuracy and convergence properties of the computational scheme are analyzed.

DOI: 10.1103/PhysRevB.70.245322

PACS number(s): 73.20.-r, 71.15.-m, 71.15.Ap

I. INTRODUCTION

Scattering of electrons by interfaces underlies a variety of experimental techniques, such as scanning tunneling^{1,2} and ballistic electron emission microscopy^{3,4} or, at higher energies, photoelectron spectroscopy⁵ and low-energy electron diffraction.⁶ Transmission coefficients of Bloch waves are the basis for understanding mesoscopic transport phenomena,^{7,8} in particular in technologically important metal-semiconductor heterojunctions or magnetic multilayers.⁹ In many applications, apart from the scattering matrix, a detailed information about wave functions is required, for example, to reveal current inhomogeneities or to calculate the photoemission matrix elements.

There exists a variety of computational approaches to the problem of electronic structure of a scattering layer sandwiched between two semi-infinite crystals. Within a wave functions approach various finite-difference real space schemes have been developed.^{4,10-14} Alternatively, a Green functions approach in a localized basis formulation is extensively employed when a direct interaction between the semi-infinite leads can be neglected.¹⁵⁻¹⁹ Both the finite-difference schemes and most of the Green function matrix techniques refer to a pseudopotential treatment of the scattering region, whereas the majority of calculations for singular (so-called all-electron) crystal potentials are performed within the Korringa-Kohn-Rostoker formalism.^{1,6,20-22}

Although the experience with band structure calculations suggests that the augmented-plane-wave (APW) representation²³ is the most direct way to achieve a high accuracy of wave functions, the applications of the APW formalism to scattering problems are still rather rare.²⁴⁻²⁹ The APW based methods employ a variational approach to the scattering wave function, with the semi-infinite substrate being represented either by its complex band structure,³⁰ as in Refs. 24-26, or by a surface inverse Green function,³¹ as in Refs. 27-29. The main difficulty in the implementation of

the APW based schemes stems from a complicated numerical representation of the basis functions—the augmented plane waves. In particular, in all these methods the scattering region is separated from the infinite space by a matching surface, and the presence of the muffin-tin spheres, in which the plane wave is modified and expressed by an angular-momentum set of numerical orbitals, requires a considerable computational effort to set up the boundary surface and determine boundary values.^{26,27}

The aim of the present work is to facilitate the application of APW's to electron scattering by mapping the variational problem onto an equivalent problem expressed in terms of usual plane waves. Similar to the majority of (augmented) plane waves based schemes,^{4,13,14,25,26} we describe semi-infinite substrates by their complex band structures, i.e., by the generalized Bloch waves, which in this paper are referred to as *partial waves*. This is rather close to the approach of Stiles and Hamann,²⁶ the main difference being that in the present method the basis set expansion in the scattering region is obtained without the intermediate step of generating the partial waves for this region. The developed formalism has no restrictions on the representation of the wave functions. In this work we use a set of energy independent APW's with extended radial basis to describe the Hamiltonian of the system: the extended linear APW method (ELAPW)³² is employed in the scattering region, and its $\mathbf{k}\cdot\mathbf{p}$ formulation^{33,34} is applied to the semi-infinite leads. Within the APW representation the accuracy can be systematically improved, so the calculations with the present method may serve as a benchmark for the quality of the scattering wave function.

The paper is organized as follows. In Sec. II we introduce the embedding setup, describe the trial function of the method, and define the variational functional. The applications are illustrated and the accuracy analysis is presented in Sec. III for the electron diffraction at the (100) and (111) surfaces of Al and Cu and in Sec. IV for the determination of three surface states on these surfaces.

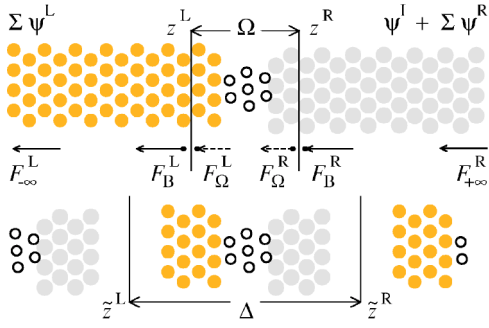


FIG. 1. (Color online) Embedding setup with a repeated slab. Upper picture: The embedded (scattering) region Ω is located between the planes z^L and z^R . The wave ψ^I is incident from the right half space, reflected waves ψ^R and transmitted waves ψ^L constitute the complex band structures of the right and the left half-spaces, respectively. The arrows represent the probability current F calculated at different $z=\text{const}$ planes; the definition is given in Sec. II B. Lower picture: The region Ω is a fragment of the slab Δ bounded by the planes \tilde{z}^L and \tilde{z}^R . The slab is repeated to form a crystal, for which a band structure problem is solved.

II. BASIC CONCEPTS

Consider two semi-infinite crystals separated by an interface region, see Fig. 1. In the embedded region Ω , between z^L and z^R , the potential is a fragment of the potential of a slab, which occupies the region Δ between the planes \tilde{z}^L and \tilde{z}^R . The slab is assumed to be thick enough, so that the slab potential V^S matches on the planes z^L and z^R , respectively, the potentials V^L and V^R of the semi-infinite substrates. We use superscripts R and L to distinguish between the two half spaces.

The system is periodic in the $\mathbf{r}^{\parallel}=(x,y)$ plane, and its stationary states are characterized by the Bloch vectors \mathbf{k}^{\parallel} parallel to the surface. In each semi-infinite crystal the potential is periodic in the surface perpendicular z direction, so the complex band structure of the half space can be introduced: for a given energy E and vector \mathbf{k}^{\parallel} a set of partial waves $\psi(k;\mathbf{r})$ —solutions of the Schrödinger equation with different surface perpendicular projections k of the Bloch vector. The set of physically relevant functions ψ comprises a finite number of propagating solutions (real k), which may travel in both directions, and an infinite number of evanescent waves (complex k), which decay to the right in the right half space and to the left in the left one.

Let us consider the scattering of a Bloch wave $\psi^I(k^I;\mathbf{r})$ traveling towards the interface from $+\infty$. In the half space $z > z^R$ the incident wave ψ^I satisfies the Schrödinger equation—it belongs to the \mathbf{k}^{\parallel} projected real band structure of the right crystal. The scattering function $\Psi(\mathbf{k}^{\parallel};\mathbf{r})$ in the right half-space is a sum of the incident wave and a number of reflected waves $\psi^R(k_n^R;\mathbf{r})$, which propagate or decay towards $+\infty$. In the left half space, it is a sum of transmitted waves $\psi^L(k_n^L;\mathbf{r})$, which propagate or decay towards $-\infty$.

All information about the embedded region Ω is contained in the (real) band structure of the *repeated* slab $\epsilon_m(\kappa)$ arising from the invariance of the system with respect to the translation by $\tilde{z}^R - \tilde{z}^L$.³⁵ Note that we are interested in the

wave function on a finite interval, between z^L and z^R , so that the solution can be represented by a Fourier series—constructing a Fourier integral $\int d\kappa$ is not required. Thus, for a given \mathbf{k}^{\parallel} one κ point is sufficient, and it is natural to choose $\kappa=0$. We denote by $\{\xi_m\}$ the set of slab eigenfunctions at this point:

$$\hat{H}^S \xi_m = \epsilon_m \xi_m. \quad (1)$$

It is essential that Ω is a subdomain of Δ because we need a basis set to reproduce a function within Ω with arbitrary boundary values on the planes z^L and z^R . Any function periodic in the interval $[\tilde{z}^L, \tilde{z}^R]$ can be expanded in a convergent series in terms of ξ_m . [We have chosen point Γ in Eq. (1), $\kappa=0$.] Obviously, in the region Ω , the scattering function Ψ can be represented by a series of the slab solutions with any desired accuracy $\Psi^\Omega = \sum_m a_m \xi_m$. Indeed, the wave function Ψ^Ω can be extended beyond Ω to the slab domain Δ so as to satisfy the same boundary conditions on the slab boundaries as the functions $\{\xi_m\}$. It should be noted that the set is overcomplete because such an extension is not unique.

An alternative approach to the representation of the scattering function in the embedded region has been developed by Stiles and Hamann in Ref. 26. There a partial wave expansion is used also in the scattering region, so that one first constructs several variational solutions ψ of the Schrödinger equation in Ω for the same energy E and then seeks a linear combination of them that minimizes the mismatch at the boundaries. The idea of the present method is to unite the two tasks into a single variational procedure with the aim to enhance the variational freedom. In other words, we exploit the property that with the same basis set $\{\xi_m\}$ the sum of partial waves may be obtained with a higher accuracy than each individual function ψ .

A. The representation of the trial function

The trial function of the method depends upon the coefficients $\{b_n^L\}$ and $\{b_n^R\}$ of the partial waves in the left and the right bulk crystals, respectively, and upon the coefficients $\{a_m\}$, which determine the wave function in the interface region

$$\Psi = \begin{cases} \psi^I + \sum_n b_n^R \psi_n^R, & z > z^R, \\ \sum_n b_n^L \psi_n^L, & z < z^L, \\ \sum_m a_m \xi_m, & z^L < z < z^R. \end{cases} \quad (2)$$

By construction the trial function satisfies the Schrödinger equation in both half-spaces, and the variational coefficients $\{a_m\}$ and $\{b_n^X\}$, $X=L$ or R , are determined by the two requirements (i) that the Schrödinger equation within Ω is satisfied

$$(\hat{H}^S - E)\Psi^\Omega = \sum_m a_m (\epsilon_m - E) \xi_m = 0 \quad (3)$$

and (ii) that the matching conditions at the boundary planes $z=z^L$ and $z=z^R$ are fulfilled:

$$\sum_m a_m \xi_m^X(\mathbf{G}^{\parallel}) = \delta_{XR} \psi^J(\mathbf{G}^{\parallel}) + \sum_n b_n^X \psi_n^X(\mathbf{G}^{\parallel}), \quad (4)$$

$$\sum_m a_m \eta_m^X(\mathbf{G}^{\parallel}) = \delta_{XR} \zeta^J(\mathbf{G}^{\parallel}) + \sum_n b_n^X \zeta_n^X(\mathbf{G}^{\parallel}). \quad (5)$$

Here the same symbols ψ and ξ are used for the components of the Laue representation of the functions, for example,

$$\xi_m(\mathbf{r}) = \frac{1}{\sqrt{A}} \sum_{\mathbf{G}^{\parallel}} \xi_m(\mathbf{G}^{\parallel}, z) e^{i\mathbf{G}^{\parallel} \cdot \mathbf{r}^{\parallel}}. \quad (6)$$

The missing argument z in Eqs. (4) and (5) means that the function is evaluated at the corresponding matching plane, for example, $\xi_m^X(\mathbf{G}^{\parallel}) \equiv \xi_m(\mathbf{G}^{\parallel}, z^X)$. The functions η_m and ζ_n are the normal derivatives $-id/dz$ of the functions ξ_m and ψ_n , respectively. The symbol δ_{XR} allows for the presence of the incident wave in the right half space: $\delta_{RR}=1$ and $\delta_{LR}=0$.

The variational procedure depends upon the answer to the question: With a finite number of partial waves ψ and basis functions ξ what is the best approximation to the function Ψ ? In the present method we require that in the region Ω the solution minimize its deviation from the true function in a least-squares sense

$$\sigma^{\Omega} = \|(\hat{H}^S - E)\Psi^{\Omega}\| \equiv \int_{\Omega} |(H^S - E)\Psi^{\Omega}|^2 d\mathbf{r}. \quad (7)$$

The functional σ^{Ω} is positive definite and quadratic in energy. Alternatively, the requirement that the function satisfies the Schrödinger equation in the embedded region can be expressed by a functional linear in energy.^{26,29} For example, if the trial function satisfies by construction the boundary conditions in value (4) the functional whose first variation at the exact solution vanishes takes the form

$$\int_{\Omega} \Psi^{\Omega*} (H^S - E) \Psi^{\Omega} d\mathbf{r} + \int_F \Psi^{\Omega*} \hat{\partial}_n \Psi^{\Omega} d\mathbf{r}^{\parallel} + \text{c.c.} \quad (8)$$

The surface integral arises from the nonrelativistic kinetic energy operator $-\Delta$ as a consequence of the arbitrariness of the derivative boundary conditions at the matching planes.

In contrast to the functional (8), the expression (7) does not involve surface terms. It gives a measure of the deviation of the trial function from the true solution in the Ω region and is easily expressed in terms of the slab eigenfunctions ξ :

$$\sigma^{\Omega} = \sum_{ij} (\epsilon_i - E)(\epsilon_j - E) \omega_{ij} a_i^* a_j. \quad (9)$$

Only the overlap integrals ω_{ij} have to be evaluated numerically:

$$\omega_{ij} = \int_{\Omega} \xi_i^*(\mathbf{r}) \xi_j(\mathbf{r}) d\mathbf{r}. \quad (10)$$

Thus, from now onwards we represent the slab by an effective Hamiltonian given by the set of its exact eigenfunctions $\{\xi_m\}$. Numerical errors in these functions distort the original Hamiltonian, which may manifest itself in a failure of stationary states to conserve current.

At the boundaries the function and derivative mismatches are

$$f^X = \int_A \left| \sum_m a_m \xi_m^X - \delta_{XR} \psi^J - \sum_n b_n^X \psi_n^X \right|^2 d\mathbf{r}^{\parallel}, \quad (11)$$

$$d^X = \int_A \left| \sum_m a_m \eta_m^X - \delta_{XR} \zeta^J - \sum_n b_n^X \zeta_n^X \right|^2 d\mathbf{r}^{\parallel}. \quad (12)$$

Here the integration is over the surface A of the 2D unit cell of the system; the argument \mathbf{r}^{\parallel} is dropped.

B. The variational method

In the exact function, the matching errors $f^{L,R}$ and $d^{L,R}$ vanish as well as the error σ^{Ω} in the embedding region [Eq. (7)], but in an approximate solution the errors cannot be simultaneously minimized because the coefficients $\{a_m\}$ enter each of the values. Thus, with a given set of functions ψ and ξ the accuracy of matching is the higher the lower is the quality of Ψ^{Ω} in the sense of Eq. (7). The two sources of error refer to spaces of different dimensionality: the 3D integral (7) for σ^{Ω} and the 2D integrals (11) and (12) for f^X and d^X . To bring the two factors to a common denominator, we shall use as a guide their influence on the current conservation in the scattering state. Because the current is an important observable it is desirable that the values of current calculated at different $z=\text{const}$ planes be in the best possible agreement. In particular, a consequence of the inaccuracy of the function Ψ^{Ω} is the difference of the fluxes F_{Ω}^R and F_{Ω}^L at the matching planes (see Fig. 1)

$$\Delta F_{\Omega} = |F_{\Omega}^R - F_{\Omega}^L|, \quad (13)$$

which are calculated from the ξ representation of Ψ^{Ω} :

$$F_{\Omega}^X = \sum_{\mathbf{G}^{\parallel}} J_{\Omega}^X(\mathbf{G}^{\parallel}). \quad (14)$$

Here J_{Ω}^L is the right-side limit of the \mathbf{G}^{\parallel} -resolved current in the \mathbf{z} direction at the left plane and J_{Ω}^R the left-side limit at the right plane:

$$J_{\Omega}^X(\mathbf{G}^{\parallel}) = \Psi^{\Omega*}(\mathbf{G}^{\parallel}, z) \left[-i \frac{d}{dz} \Psi^{\Omega}(\mathbf{G}^{\parallel}, z) \right] \Big|_{z=z^X} + \text{c.c.}$$

In principle, ΔF_{Ω} can be made arbitrarily small by reducing σ^{Ω} . Similarly, the residual mismatch at the boundaries can be characterized by a value that has the dimension of flux

$$\Delta F_M = \left\{ \sum_X \sum_{\mathbf{G}^{\parallel}} [J_{\Omega}^X(\mathbf{G}^{\parallel}) - J_B^X(\mathbf{G}^{\parallel})]^2 \right\}^{1/2}. \quad (15)$$

Here J_B^L is the left-side limit of the current at the left plane and J_B^R the right-side limit at the right plane.

To find the solution Ψ , we minimize the functional

$$\Phi = \sigma^{\Omega} + W \sum_X [f^X + d^X], \quad (16)$$

which vanishes with its first variation at the exact solution, and which depends upon a factor W that balances the errors

coming from the failure to pointwise satisfy the Schrödinger equation in the Ω region and to pointwise match the ξ expansion to the ψ expansions at the boundaries. The value of W is determined automatically within the variational procedure. We start with an excessively large W , so that the mismatches at the boundaries are minimized without taking care of the shape of the function inside Ω . Owing to the abundant number of the ξ functions, the flux mismatch ΔF_M [Eq. (15)] is negligible. By gradually reducing W we relax the requirement of matching, and at certain point ΔF_M starts growing and may exceed the current value of ΔF_Ω . The optimal value of W is determined by the requirement that ΔF_M be close to ΔF_Ω . Of course, this criterion is applied only if ΔF_M exceeds a physically reasonable limit of accuracy, say, 0.1% of the incident current—otherwise W may be further reduced and Ψ^Ω further refined.

We do not introduce different weights for f^X and d^X and rely upon the variational freedom of the basis set, which will provide an optimal mismatch in one of the values (function or derivative) and an excessively small one in the other. In our calculations the optimal value of W varied with energy within two orders of magnitude, which reflects the fact that for a given energy the quality of the variational wave function is stable to considerable variations of this parameter.

It should be noted that it is not the aim of the above procedure to minimize the current nonconservation ΔF_Ω across the embedded region. In fact, it would be misleading to impose such a requirement because a less accurate function Ψ^Ω may provide a better agreement between the currents at the two surfaces. This is just a way to find a reasonable value for the parameter W . How small the actual values of ΔF_M and ΔF_Ω are depends upon the number and the quality of the basis functions ξ . We address this issue in Sec. III B.

C. Overcompleteness of the basis set

The functions ψ and ξ play different role in the variational method. The number of the partial waves ψ cannot be unrestrictedly increased: irrespective of the method of calculation only a limited number of them, those with sufficiently small decay constants $\text{Im } k$, can be calculated with acceptable accuracy. However, because the contribution from the evanescent states is the smaller the further the matching planes z^L and z^R are placed from the interface region, we can always restrict ourselves to a finite number of ψ 's without loss of accuracy. On the other hand, we must be able to generate with desired accuracy an arbitrarily large number of the slab eigenfunctions ξ . In the present work they are calculated with the extended linear augmented plane waves method.³²

The differentiation of the functional (16) with respect to the coefficients a_m , b_n^L , and b_n^R leads to a system of linear equations with a right-hand side arising from the values of function and derivative of the incident wave at the boundary z^R . As a result of the nonuniqueness of the ξ expansion of the function Ψ^Ω , the determinant of the system may turn out to be too small, which would lead to numerical instabilities in the computer implementation of the method. This problem stems from the basic idea to expand a function with un-

known boundary conditions in terms of a basis set and is common to all variational embedding methods. In the present method as well as in the method of Inglesfield and Benesh²⁹ it arises from the fact that the domain over which the basis functions are defined is larger than the embedding domain. In the method of Stiles and Hamann²⁶ the domain of the function to be found $f(z)$ coincides with the domain of the basis functions ξ_m . The function is then represented by a discretization of the Fourier integral over the 1D Brillouin zone:

$$\sum_m \int_{\text{BZ}_\perp} f_m(\kappa) \xi_m(\kappa, z) d\kappa \rightarrow \sum_m \sum_\kappa f_m(\kappa) \xi_m(\kappa, z).$$

Again, the finer is the sampling of the κ interval the more accurate is the representation, and the less stable is the numerical procedure. In Ref. 26 the authors had to restrict the summation over κ to two points.

The basis set $\{\xi_m\}$ is overcomplete in Ω , but it is complete and orthogonal by construction in Δ . Thus, the computational procedure will be protected from the instability if we formulate the problem in the domain Δ . With this aim we modify the functional (16) so as to include a requirement that the function Ψ^Ω satisfies the Schrödinger equation not only in Ω but everywhere in Δ :

$$\Phi = \sigma^\Omega + P\sigma^\Delta + W \sum_X [f^X + d^X], \quad (17)$$

where the new parameter P determines the accuracy with which the additional requirement will be fulfilled. The energy deviation σ^Δ is an integral over Δ similar to σ^Ω in Eq. (7). The minimal value of P depends upon the numerical precision of the calculations, and it is determined from the condition that the matrix in the left-hand side of the system of linear equations be positive definite with the machine precision. Thus, as a result of the number and character of the partial waves ψ varying with energy, the accuracy of the scattering function varies, and for a given energy it is the highest possible accuracy. The orthogonality of the basis functions in Δ makes the procedure absolutely stable.

D. Plane-wave formulation

Computationally, apart from the linear algebra, the method involves generating the Laue expansion of all the constituents at the matching planes [Eqs. (4) and (5)] and evaluating the overlap integrals (10). The calculations are simple and fast if the functions ψ and ξ are given in a plane wave representation, but they become very cumbersome in an APW representation, especially when the matching plane intersects the muffin-tin spheres.³⁶ (For the purpose of the numerical accuracy of functions ψ and ξ the spheres should be as large as possible.) It would be impracticable to straightforwardly expand an all-electron wave function in a Fourier series because it would result in an enormous number of Fourier coefficients, especially when localized functions are involved, such as d states of transition or noble metals.

We shall now describe a general method to solve the variational equation $\delta\Phi=0$ in a plane-wave representation. We replace the requirement $(\hat{H}^S - E)\Psi^\Omega=0$ with an equiva-

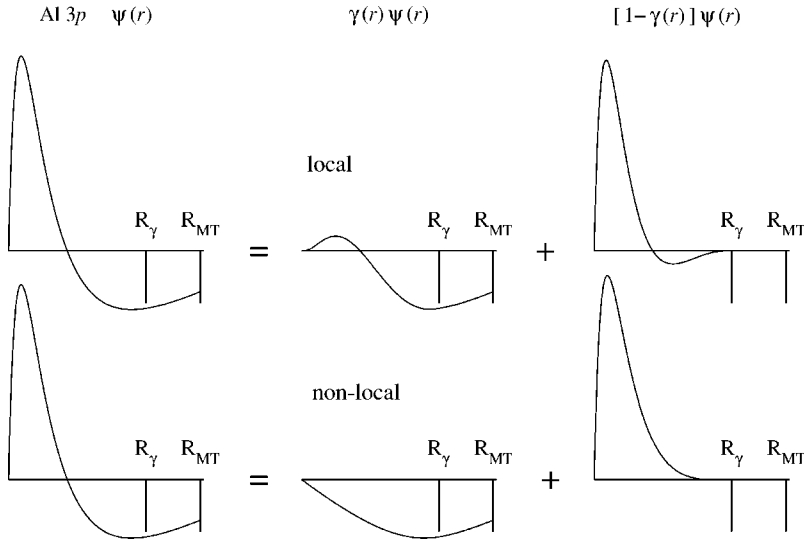


FIG. 2. Two forms of the $\hat{\gamma}$ transformation applied to the Al 3p orbital. Upper graphs: multiplication by a function $\gamma(r)$. Lower graphs: replacement by a linear combination of the free-space zero-energy solution r^l and its energy derivative r^{l+2} .

lent requirement $\hat{\gamma}(\hat{H}^S - E)\Psi^\Omega = 0$, where $\hat{\gamma}$ is an operator such that for an arbitrary function ϕ the norm $\|\hat{\gamma}\phi\|$ is zero if and only if $\|\phi\|$ is zero. Because we have assumed that the functions ξ_m pointwise satisfy the Schrödinger equation, we need only to replace the integrals ω_{ij} in Eq. (9) by the integrals

$$\tilde{\omega}_{ij} = \int_{\Omega} [\hat{\gamma}\xi_i(\mathbf{r})]^* \hat{\gamma}\xi_j(\mathbf{r}) d\mathbf{r}. \quad (18)$$

The operator $\hat{\gamma}$ is chosen such that the functions $\hat{\gamma}\xi_m$ have a rapidly convergent plane-wave expansion. Thus, the problem is formulated in terms of plane waves without resorting to pseudopotentials.

Two forms of the operator $\hat{\gamma}$ have been tried in this work. In both cases the operator modifies the function only in a close vicinity of the nuclei, see Fig. 2: inside a sphere of radius R_γ it replaces the rapidly oscillating radial functions with smoother functions and makes the entire wave function amenable to being Fourier transformed. The matching plane may then cut through the muffin-tin sphere, but it should not, in general, intersect the γ sphere. In the first case the wave function is multiplied by a positive definite function $\gamma(r)$ that depends only upon the distance from the nucleus and gradually decreases from unity at $r=R_\gamma$ to zero at $r=0$.³⁷ In the second case $\hat{\gamma}$ is a nonlocal operator: it replaces the radial function of the l th orbital in the angular momentum expansion by a linear combination of the free-electron zero-energy solution r^l and its energy derivative r^{l+2} that matches the original radial function in value and in slope at $r=R_\gamma$. The nonlocal operator removes the oscillations more efficiently, and one can achieve a better convergence of the plane wave expansion than with a simple multiplication, however, with R_γ between 1.5 and 1.9 a.u. and with about 1000 plane waves per atom the results by the two operators turned out practically identical. The local operator has an advantage that the matching plane may also cut through the γ sphere, provided that the same function $\gamma(r)$ is used in the substrate and in the slab. In this case a γ image of the function in the substrate is matched to its γ image in the embedded region,

which is legitimate because there is a one-to-one correspondence between the function and its image. Of course, the values F_Ω^L and F_Ω^R in Eqs. (13) and (14) do not have the meaning of current in this case, and their exact values are not necessarily equal.

The performance of the method depends both upon the quality of the variational functions ξ_m (we have assumed that they pointwise satisfy the Schrödinger equation) and upon the quality of the plane-wave expansion, which determines the accuracy of the overlap integrals (18). In the next section we present calculations on the low energy electron diffraction with the present method and demonstrate its accuracy and convergence properties.

III. SPECIAL CASE: LEED

Diffraction of electrons at very low energies is a simple and instructive application of the method. The incident electron comes from the vacuum and the scattering function depends upon the two parameters \mathbf{k}^\parallel and E . The incident wave is normalized to a unity current, and the current carried by the scattering function is the transmitted current $T(\mathbf{k}^\parallel, E)$. We shall restrict ourselves to $\mathbf{k}^\parallel = 0$ and concentrate on the energy dependence of the transmission coefficient $T(E)$ over an energy interval up to 50 eV above the vacuum level. By scanning a wide energy interval we encounter partial waves ψ_n^L of very different character and can compare the performance of the method in different situations.

A. Methodology

In the case that the right half-space is vacuum the partial waves ψ^R are simply plane waves, and it is convenient to slightly reformulate the problem, namely, to match the function Ψ^Ω exactly over the plane $z=z^R$ to its vacuum representation.³⁸ The trial function in the vacuum half-space may now violate the Schrödinger equation, and the corresponding energy deviation is included into σ^Ω : the integral in Eq. (7) extends to the vacuum half-space, but the mismatches f^R and d^R vanish. This is achieved by smoothly continuing

the Laue decomposition (6) of each function ξ_m to the vacuum. To each function $\xi_m(\mathbf{G}^{\parallel}, z)$ a linear combination of two functions is attached at $z=z^R$: the vacuum solution

$$\psi_{\mathbf{G}^{\parallel}}^R(\mathbf{r}^{\parallel}, z) = \exp[i(\mathbf{G}^{\parallel} + \mathbf{k}^{\parallel})\mathbf{r}^{\parallel} + ik^{\perp}z],$$

with $|\mathbf{G}^{\parallel} + \mathbf{k}^{\parallel}|^2 + k^{\perp 2} = E$, and an auxiliary function

$$a_{\mathbf{G}^{\parallel}}^R(\mathbf{r}^{\parallel}, z) = \exp[i(\mathbf{G}^{\parallel} + \mathbf{k}^{\parallel})\mathbf{r}^{\parallel} + iq^{\perp}z],$$

with $|\mathbf{G}^{\parallel} + \mathbf{k}^{\parallel}|^2 + q^{\perp 2} = E_{\text{aux}}$ and $\text{Re } q^{\perp} = 0$. The auxiliary energy E_{aux} is taken considerably lower than E , so that the auxiliary functions decay fast into the vacuum. For $\mathbf{G}^{\parallel} = 0$ the solution ψ_0^R is always propagating: it is the outgoing plane wave (specular beam). The functions ξ_m are thereby defined in the entire half-space $z > z^L$.

The free term has to be modified too: unlike in Eq. (2), it is not just the incident wave

$$\psi^I(\mathbf{r}^{\parallel}, z) = \frac{1}{\sqrt{2k^I}} \exp[i\mathbf{k}^{\parallel} \cdot \mathbf{r}^{\parallel} - ik^I z],$$

but a linear combination with the outgoing and the auxiliary wave

$$\rho^I(\mathbf{r}^{\parallel}, z) = \psi^I(\mathbf{r}^{\parallel}, z) + c_0 \psi_0^R(\mathbf{r}^{\parallel}, z) + c_{\text{aux}} a_0^R(\mathbf{r}^{\parallel}, z),$$

where the coefficients c_0 and c_{aux} are defined by the condition that the function ρ^I vanishes with vanishing derivative at $z=z^R$. Thus, the trial function is smoothly continuous in the half-space $z > z^L$ and it satisfies the Schrödinger equation both in the bulk half space $z < z^L$ and far from the surface in the vacuum:

$$\Psi = \begin{cases} \rho^I + \sum_m a_m \xi_m, & z > z^L, \\ \sum_n b_n^L \psi_n^L, & z < z^L. \end{cases} \quad (19)$$

By exactly matching the trial function at the surface z^R we get rid of the variational coefficients b_n^R [see Eq. (2)]. In the exact solution the auxiliary functions $a_{\mathbf{G}^{\parallel}}^R$ coming from ρ^I and from all of the ξ_m cancel each other out.

In the left half-space, the complex band structure constituents ψ_n^L are calculated with the inverse extended linear augmented plane waves $\mathbf{k} \cdot \mathbf{p}$ method.³³ The solution of the Schrödinger equation with a Bloch vector k_n is a product of the exponential factor $\exp[i(k_n - k_0)z]$ and a Bloch function $\phi_n^{k_0}$ with the reference Bloch vector k_0 . The latter is given in terms of APW's χ_i at the reference point $\mathbf{k}^{\parallel} + \mathbf{z}k_0$:

$$\phi_n^{k_0} = \sum_i C_i \chi_i(\mathbf{k}^{\parallel} + \mathbf{z}k_0, \mathbf{r}).$$

In the $\mathbf{k} \cdot \mathbf{p}$ method the coefficients $\{C_i\}$ describe the partial wave ψ_n^L over the whole half space, whereas in other (augmented) plane-wave based methods^{13,26,28} the complex band structure is constructed one layer at a time, and a piecewise representation of ψ 's is used. As has been mentioned in Sec. II C, in variational methods this leads to an overcompleteness of the bases set. On the other hand, in the $\mathbf{k} \cdot \mathbf{p}$ method, additional computational effort is required to accurately de-

scribe the wave function in the muffin-tin spheres: a special extension of the radial basis set has to be introduced, as explained in Ref. 34.

The $\{\xi_m\}$ set comprises the slab states from the bottom of the valence band to a cutoff energy E_{ξ} . The localized atomiclike states should not be included because they are orthogonal to all scattering functions. The cutoff energy E_{ξ} determines the accuracy of the calculation and it depends both upon the thickness of the slab Δ (see Fig. 1) and the relative thickness of the embedded region

$$\theta = (z^R - z^L)/(z^R - z^L). \quad (20)$$

For a given energy E , the cutoff energy is the lower the thicker the slab and the thinner the embedded layer. In the present calculations the slabs that modeled the (100) and (111) surfaces of Al and Cu were 40–50 a.u. thick, and with θ between 0.1 and 0.6 the convergence at a given energy E was achieved with E_{ξ} some 15 to 30 eV above the energy E .

B. Transmission spectra

The electron transmission spectra for (100) and (111) surfaces of Al and Cu are shown in Fig. 3. The lower curves are obtained with a realistic self-consistent potential at the surface, and the upper curves with a steplike potential (see Fig. 4), so that a few layers of the bulk crystal are embedded between the vacuum (constant potential) and the bulk half spaces. The steplike potential is computationally the more demanding because both matching planes are close to the nuclei and the boundary values $\xi_m^R(\mathbf{G}^{\parallel})$ and $\eta_m^R(\mathbf{G}^{\parallel})$ of large G^{\parallel} are involved [see Eqs. (4) and (5)]. The steplike setup enables us to check the calculations by comparing the upper curves to a calculation without the embedding region, i.e., bulk is matched immediately to vacuum, in which case the new formalism connected to the functions ξ is not involved. In all the four cases the curves virtually pointwise coincided with the curves by the embedding method. This proves that the equations $(\hat{H}^S - E)\Psi^{\Omega} = 0$ and $\hat{\gamma}(\hat{H}^S - E)\Psi^{\Omega} = 0$, see Sec. II D, are equivalent not only mathematically but also computationally. The calculations on copper are an especially stringent test of the plane-wave formulation of the energy minimization problem (7). The presence of the 3d states in the ξ set is perfectly dealt with by the $\hat{\gamma}$ operator, and we observe no difference in performance between Al and Cu.

At low kinetic energies the steplike potential reduces transmission for all the four surfaces. It is seen in Fig. 4 that the same ψ wave transmits current into the bulk, but the wave function in vacuum depends strongly on the shape of the potential barrier. On the contrary, in the vicinity of the gaps in the \mathbf{k}^{\parallel} projected band structure the smooth potential barrier may increase the reflection, which is seen, for example, in the (111) spectra in Fig. 3 for Al at around 20 eV and for Cu at 30 eV.

The thickness of the lines in Fig. 3 arises from vertical error bars, which characterize the current nonconservation in the scattering function. In terms of the notation in Fig. 1 and in Eqs. (13) and (14) the length of the bar is

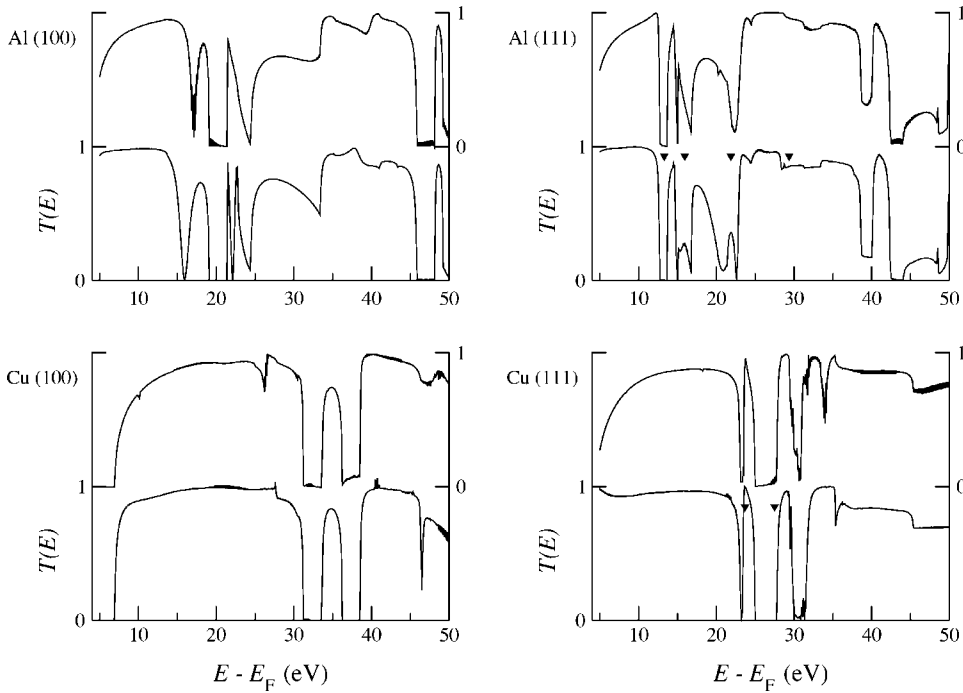


FIG. 3. Normal incidence electron transmission spectra for (100) and (111) surfaces of Al and Cu. Upper curves are calculated with a steplike surface potential barrier, and lower curves with a realistic potential, see Fig. 4. Vertical error bars, which characterize the current nonconservation in the LEED function according to Eq. (21), produce a finite width of the lines. The locations of the minima in the $T(E)$ spectra of the (111) surfaces of Al and Cu experimentally observed in Ref. 39 are shown by triangles.

$$[(F_B^R - F_{+\infty}^R)^2 + (F_\Omega^L - F_\Omega^R)^2 + \Delta F_M^2]^{1/2}. \quad (21)$$

Note that $F_\Omega^R = F_B^R$ and that only the left boundary contributes to the mismatch ΔF_M defined in Eq. (15). The method is seen to provide a good current conservation over a wide energy range in all the cases studied.

It should be noted that the error minimized by the variational procedure—expressed by the functional (16)—is rather loosely connected to the uncertainty of the observable $T(E)$. In particular, the error bars in Fig. 3 do not give the limits for the value of $T(E)$. The effect of the residual errors in the scattering function on the transmission coefficient is revealed by the dependence of the spectra on the position of the matching plane z^L . For each of the surfaces a series of calculations was performed with different z^L placed midway between adjacent atomic planes (see Fig. 4). For the functions ψ all these planes are equivalent because to within a Bloch factor they have the periodicity of the interlayer spacing. The same is true for the (well-converged) ξ functions, at

least for the steplike potential barrier, for the reasons of symmetry.

When the left matching plane moves leftwards the embedded region widens and the variational task is thereby redistributed between ψ 's and ξ 's. At the same time, different cross sections of the scattering function are probed, which are not necessarily equivalent.

The effect of the thickness θ on the accuracy of the wave function is determined by the two competing factors.

(i) For a thin embedded region, the nearest vicinity of the surface is described by the set of the partial waves ψ , and steeply decaying ψ 's may contribute to the wave function. If such waves are not included in the set the accuracy would suffer (see the first paragraph of Sec. II C). As the embedded region gets thicker such waves are taken into account by the ξ expansion, and the accuracy improves.

(ii) On the other hand, the variational freedom of the ξ set reduces as θ grows, and the accuracy of the ξ expansion deteriorates.

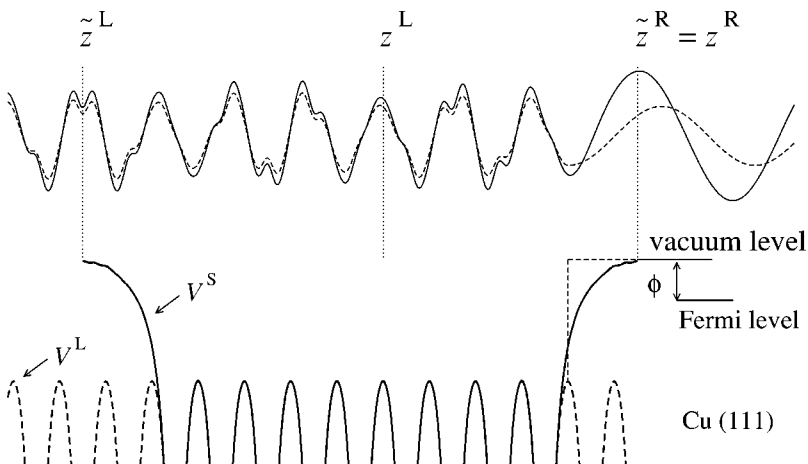


FIG. 4. Scattering of the plane wave with kinetic energy 1.6 eV by a Cu (111) crystal surface with a realistic potential barrier (full line) and with a steplike barrier (dashed line). In the lower graph the self-consistent potential of the slab V^S is superimposed on the self-consistent potential of the bulk crystal V^L . The work function was taken $\phi = 4.94$ eV as cited in Ref. 42. In the upper graph the real part of the $\mathbf{G}^{\parallel} = 0$ Fourier component of the function $\gamma\Psi$ is shown for the realistic and for the steplike potential by the full and the dashed line, respectively. The vertical lines show the location of the matching planes z^L and z^R , which bound the embedded region Ω , and the planes \tilde{z}^L and \tilde{z}^R , which bound the slab domain Δ .

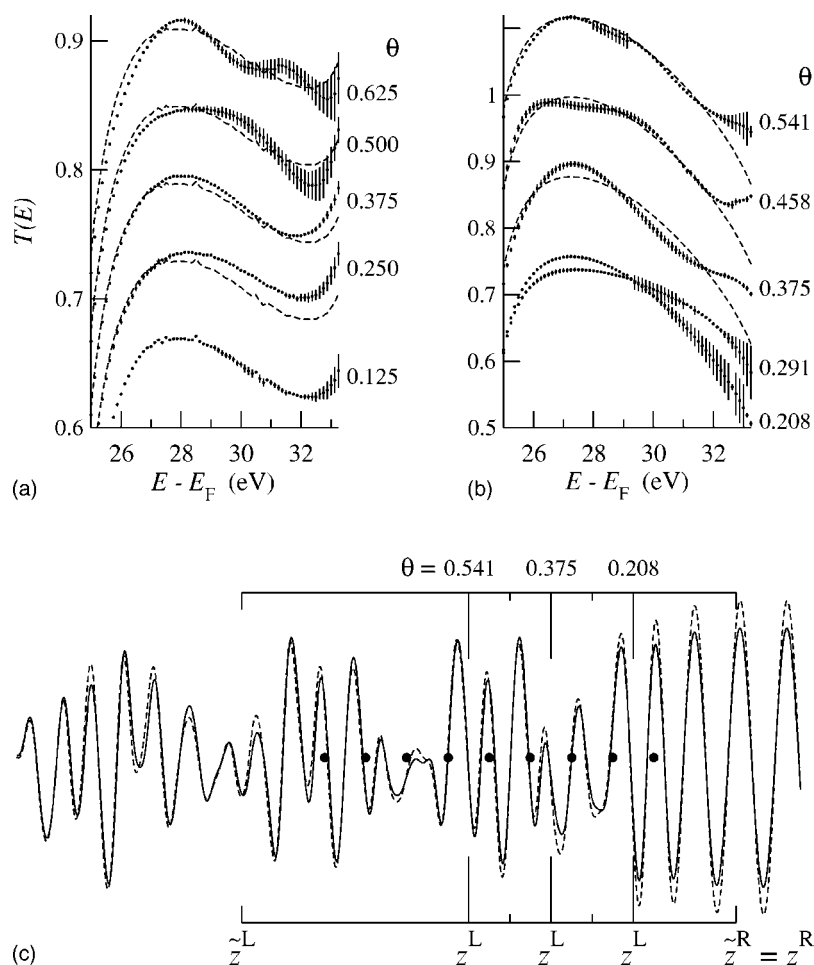


FIG. 5. Upper graphs: Normal incidence Al (100) electron transmission spectra for $E - E_F$ between 25 and 33 eV for the steplike potential barrier (a) and for the realistic barrier (b) for several thicknesses θ of the embedded region. The curves are vertically shifted with a step of $\Delta T = 0.06$ in graph (a) and $\Delta T = 0.12$ in graph (b). For comparison the $\theta = 0.125$ curve is repeated as a dashed line in graph (a) and the $\theta = 0.208$ curve in graph (b). The length of the vertical error bars is defined by Eq. (21); in graph (b) the error bars are four times magnified. Lower graph: The real part of the $\mathbf{G}^{\parallel} = 0$ component of the function $\gamma\Psi$ at the energy $E - E_F = 32.5$ eV for $\theta = 0.208$ (full line) and for $\theta = 0.375$ (dashed line). Solid circles show the nine atomic layers that constitute the slab. The right matching plane z^R is kept 7.7 a.u. away from the outermost atomic layer, and the left matching plane z^L is taken at five different positions between the layers.

In the range of θ from 0.1 to 0.6 all the eight curves were found rather stable: the variations of $T(E)$ almost never exceeded 2%. The strongest dependence on the location of the matching plane is observed in the interval between 26 and 33 eV in the Al (100) spectrum, see Figs. 5(a) and 5(b). The transmission coefficient is seen to oscillate as a function of θ both for the steplike (a) and for the realistic (b) potential barrier. Surprisingly, in the latter case the current conservation criterion (21) is fulfilled with extremely high accuracy for all θ . The reason for the non-steady behavior of $T(E)$ is that the wave function is very strongly modulated, see Fig. 5(c); in this energy interval two Bloch functions with different Bloch vectors contribute equally strongly to the scattering function. As a result, at certain locations of the matching plane the numerical errors in boundary values of the ψ and ξ add up, which affects the output $T(E)$. Unexpectedly, in this case the uncertainty of the wave function coexists with very small values of the criterion (21). In other words, the “incorrect Hamiltonian” given by its exact eigenfunctions ξ may provide a perfect current conservation.

We infer from the above analysis that the limitations of the present procedure stem from the limited accuracy of constituents ψ and ξ rather than from the convergence properties of the procedure. The functions ψ and ξ are calculated with a variational method, so the errors in boundary values are unavoidable. Nevertheless, even in such difficult cases, the uncertainty of the wave function is not dramatic [see Fig. 5(c)],

and the accuracy achieved is acceptable in many applications.

Experimentally, the $T(E)$ curves are obtained by means of low-energy-electron reflectance³⁹ or target current⁴⁰ spectroscopy. The \mathbf{k}^{\parallel} projected gaps of the real band structure are reflected as minima in the $T(E)$ spectra, but some minima may have a more complicated origin.³⁸ In Fig. 3 the minima in the (111) spectra of Al and Cu observed in Ref. 39 are shown by triangles. The sharpness of experimentally observed structures may provide information about the inelastic scattering of the incident electron, and such information can be extracted from the experiment by simulating the inelastic effects with an energy dependent imaginary potential $-iV_i$ added to the Hamiltonian.⁴¹

IV. SURFACE STATES

The calculation of surface states provides a complimentary test of the embedding method. Now the incident wave is absent, and one looks for the energy at which a solution exists that is spatially localized in the z coordinate. The determination of the surface state proceeds as follows: for a sufficiently thick embedded region the surface state in the bulk $z < z^L$ can be represented by a single evanescent wave $\psi^L(\mathbf{r})$, which delivers the boundary constraints on the value of the function $\Psi^{\Omega}(\mathbf{r})$ at $z = z^L$ [see Eq. (4)]:

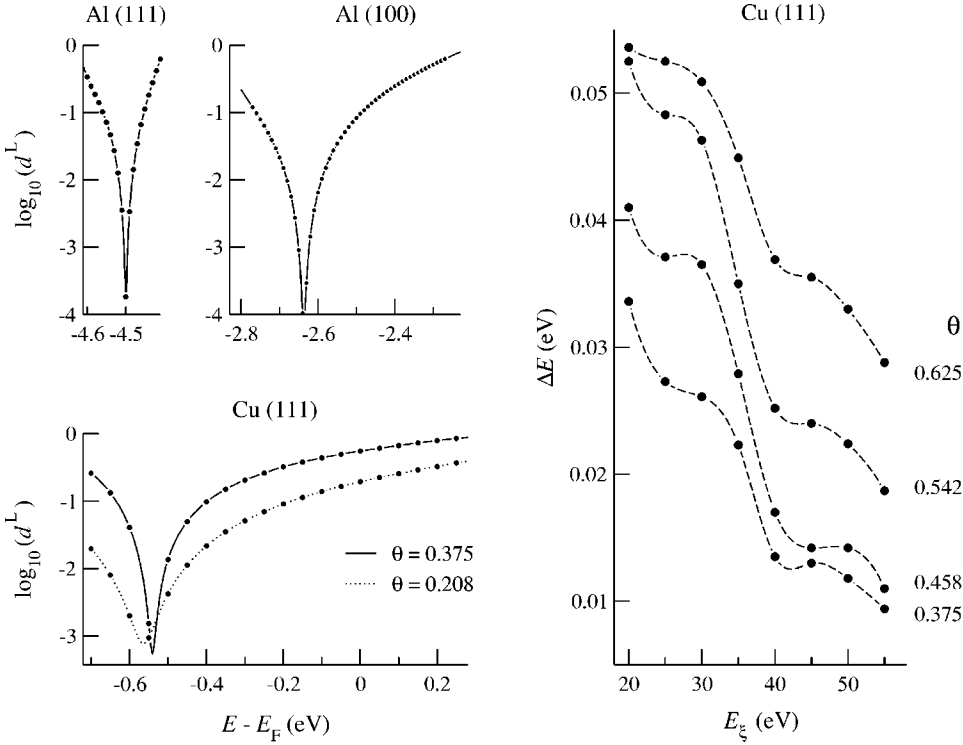


FIG. 6. The three left graphs show the energy dependence of the derivative mismatch d^L [Eq. (24)] between the solution Ψ^Ω of the boundary value problem and the evanescent state ψ^L within the gaps of the $\mathbf{k}^\parallel=0$ projected real band structure for three surfaces. The right graph shows for the Cu (111) surface state at $E - E_F = -0.55$ eV the dependence of the energy deviation $\Delta E = \sqrt{\sigma^\Omega}$ of the variational wave function upon the energy cutoff E_ξ of the basis set for four thicknesses θ of the embedded region.

$$\sum_m a_m \xi_m^L(\mathbf{G}^\parallel) = \psi^L(\mathbf{G}^\parallel). \quad (22)$$

The derivative of the function $\Psi^\Omega(\mathbf{r})$ is free. The second boundary condition is given by the exponential decay of the function at $z \rightarrow +\infty$. For a given energy E , the solution of the boundary value problem in the half-space $z > z^L$ is unique. It is obtained by solving the variational equation $\delta \|\gamma(\hat{H}^S - E)\Psi^\Omega\| = 0$ under the given boundary constraints. Then, the energy is sought at which the function turns out smooth at $z = z^L$, i.e., the derivative condition is satisfied [see Eq. (5)]:

$$\sum_m a_m \eta_m^L(\mathbf{G}^\parallel) = \zeta^L(\mathbf{G}^\parallel). \quad (23)$$

The energy dependence of the derivative mismatch

$$d^L = \int_A \left| \sum_m a_m \eta_m^L - \zeta^L \right|^2 d\mathbf{r}^\parallel \quad (24)$$

for three surface states on Al (100) and Al and Cu (111) surfaces is shown in Fig. 6. The derivative mismatch drops by three orders of magnitude over several tenths of eV, and the minimum gives the surface state energy.

Similar to the scattering problem [see Eq. (17)] the value to be minimized is

$$\Phi = \sigma^\Omega + P\sigma^\Delta + Wf^L. \quad (25)$$

The factor W is chosen such that the normalized boundary value mismatch

$$\mu = \int_A \left| \sum_m a_m \xi_m^L - \psi^L \right|^2 d\mathbf{r}^\parallel, \quad \text{with} \quad \int_A |\psi^L|^2 d\mathbf{r}^\parallel = 1,$$

is kept below certain border, typically $\mu < 0.001$.

The surface state energy converged very fast with the number of basis functions and was rather stable to the thickness of the embedding region. Because the matching is thought sufficiently accurate the quality of the wave function is characterized by the energy deviation σ^Ω . Owing to the competition of the surface and the bulk contributions to the functional Φ , the deviation σ^Ω does not, in general, steadily reduce with extending the basis set (increasing the cutoff energy E_ξ). However, for a sufficiently thick embedding region the main contribution to the functional comes from the bulk integral, and the energy deviation decreases steadily with increasing the energy cutoff, see right panel of Fig. 6.

The calculations described in this section were the basis for the recent study of the photoemission from the surface states on the (100) and (111) Al surfaces.⁴³ Accurate determination of both the surface state and the photoelectron final states made it possible to explain the photon energy dependence of the photoemission intensity.

V. CONCLUDING REMARKS

The full-potential all-electron embedding method developed in this paper reduces the scattering problem for the interface to solving the band structure problem for each of the constituents: two semi-infinite leads and a slab containing the scattering region. This variational method is based on a partial waves (complex band structure) representation of the wave function in semi-infinite leads and a complete-basis (real band structure) representation in the scattering region. To circumvent the problem of overcompleteness of the basis set, the variational problem is formulated in terms of orthogonal functions by imposing an additional requirement on the trial function.

The variational functional combines the requirement that the function satisfies the Schrödinger equation in the scattering region (expressed by a volume integral) and that it is smoothly continuous at the boundaries (surface integral). Current-conservation considerations are used to judge on the relative importance of the two requirements and to control the accuracy with which they are fulfilled. An attractive feature of the positive-definite form $\|(\hat{H}-E)\Psi\|$ of the volume contribution is that it leads to a Hermitean matrix: the kinetic energy operator does not generate surface terms in the first variation of this functional—in contrast to a functional linear in energy. This is especially convenient in semirelativistic calculations, where the kinetic energy operator has a more complicated form and the surface contribution from the mass-velocity term has to be taken into account when a boundary plane comes close to the nuclei. Owing to the absence of the surface terms, the present formalism can be straightforwardly applied in semirelativistic calculations, for example, with the energy-dependent Hamiltonian of Koelling and Harmon⁴⁴ or with the Foldy-Wouthuysen Hamiltonian.³⁴ It should be noted that the semirelativistic corrections may lead to a violation of current conservation, which is an essential ingredient of the present scheme. The experience shows, however, that for moderately large atomic numbers (at least up to Au) the nonrelativistic current is transferred from one matching plane to another with a physically acceptable accuracy.

To facilitate the numerical implementation of the method, a plane-wave representation of the basis functions is introduced. This enables us to discard unphysical computational parameters, such as muffin-tin spheres radii or energy parameters E_v , at the stage of computing the scattering wave function, and to strongly simplify the geometrical aspects of the calculation. In order to be able to use the plane-wave formalism, we transfer from the original Schrödinger equation in the embedded region $(\hat{H}-E)\Psi^\Omega=0$ to an equivalent equation $\hat{\gamma}(\hat{H}-E)\Psi^\Omega=0$, with the role of the operator $\hat{\gamma}$ being to damp

the oscillations of the wave function near the nucleus. The equivalence of the two equations in practical calculations is proved by the test calculations for a steplike potential barrier, i.e., by embedding a fragment of the periodic bulk crystal, which can be directly compared to the calculations without an embedding region. The output of the variational procedure are the coefficients $\{b_n^{L,R}\}$ of the partial waves $\psi_n^{L,R}$ in the semi-infinite crystals and the coefficients $\{a_m\}$ of the slab eigenfunctions ξ_m . Because both ψ 's and ξ 's are originally given in the APW representation one immediately recovers the APW representation of the scattering function.

The convergence properties of the method have proved very favorable: both the required $\text{Im } k$ range of the partial waves ψ and the energy range E_ξ of the basis functions ξ are accessible by routine (complex) band structure calculations. The accuracy limitations of the method stem from numerical errors in the basis functions. An essential assumption of the formalism is that they are exact solutions of a Schrödinger equation, and because in practice they are obtained with a variational method (ELAPW in this work) the failure of the basis functions to pointwise satisfy the Schrödinger equation may lead to uncertainties in the scattering wave function. Nevertheless, even in the most difficult cases considered the accuracy was quite acceptable. The current conservation analysis of the transmission spectra and the determination of surface states on Al and Cu surfaces prove the efficiency and versatility of the method. The simplicity of the plane wave formulation of the variational problem combined with the most accurate APW representation of the wave functions makes the present scheme promising in a wide range of applications involving electron scattering.

ACKNOWLEDGMENTS

I would like to thank W. Schattke and A. Perlov for helpful discussions. This work was supported by Deutsche Forschungsgemeinschaft (Forschergruppe FOR 353).

-
- ¹G. Doyen, D. Drakova, and M. Scheffler, Phys. Rev. B **47**, 9778 (1993).
²H. Ness and A. J. Fisher, Phys. Rev. B **56**, 12 469 (1997).
³M. D. Stiles and D. R. Hamann, Phys. Rev. Lett. **66**, 3179 (1991).
⁴K. Kobayashi, Phys. Rev. B **59**, 13 251 (1999).
⁵P. J. Feibelman and D. E. Eastman, Phys. Rev. B **10**, 4932 (1974).
⁶J. B. Pendry, *Low Energy Electron Diffraction* (Academic Press, London, 1974).
⁷Y. Imry and R. Landauer, Rev. Mod. Phys. **71**, S306 (1991).
⁸D. S. Fisher and P. A. Lee, Phys. Rev. B **23**, 6851 (1981).
⁹P. Weinberger, Phys. Rep. **377**, 281 (2003).
¹⁰J. A. Appelbaum and D. R. Hamann, Phys. Rev. B **6**, 1122 (1972).
¹¹K. Hirose and M. Tsukada, Phys. Rev. B **51**, 5278 (1995).
¹²S. Lorenz, C. Solterbeck, W. Schattke, J. Burmeister, and W. Hackbusch, Phys. Rev. B **55**, R13 432 (1997).
¹³H. J. Choi and J. Ihm, Phys. Rev. B **59**, 2267 (1999).
¹⁴Y. Fujimoto and K. Hirose, Phys. Rev. B **67**, 195315 (2003).
¹⁵P. Krüger and J. Pollmann, Phys. Rev. B **38**, 10 578 (1988).
¹⁶J. Taylor, H. Guo, and J. Wang, Phys. Rev. B **63**, 245407 (2001).
¹⁷M. Brandbyge, J.-L. Mozos, P. Ordejón, J. Taylor, and K. Stokbro, Phys. Rev. B **65**, 165401 (2002).
¹⁸K. S. Thygesen, M. V. Bollinger, and K. W. Jacobsen, Phys. Rev. B **67**, 115404 (2003).
¹⁹A. Calzolari, N. Marzari, I. Souza, and M. Buongiorno Nardelli, Phys. Rev. B **69**, 035108 (2004).
²⁰J. M. MacLaren, X.-G. Zhang, W. H. Butler, and X. Wang, Phys. Rev. B **59**, 5470 (1999).
²¹N. Papanikolaou, J. Opitz, P. Zahn, and I. Mertig, Phys. Rev. B **66**, 165441 (2002).
²²P. Mavropoulos, N. Papanikolaou, and P. H. Dederichs, Phys. Rev. B **69**, 125104 (2004).
²³J. C. Slater, Phys. Rev. **51**, 846 (1937).
²⁴G. Wachutka, Phys. Rev. B **34**, 8512 (1986).
²⁵W. Hummel and H. Bross, Phys. Rev. B **58**, 1620 (1998).

- ²⁶M. D. Stiles and D. R. Hamann, Phys. Rev. B **38**, 2021 (1988).
- ²⁷H. Ishida, Phys. Rev. B **63**, 165409 (2001).
- ²⁸D. Wortmann, H. Ishida, and S. Blügel, Phys. Rev. B **65**, 165103 (2002).
- ²⁹J. E. Inglesfield and G. A. Benesh, Phys. Rev. B **37**, 6682 (1988).
- ³⁰V. Heine, Proc. Phys. Soc. London **81**, 300 (1963).
- ³¹J. E. Inglesfield, J. Phys. C **14**, 3795 (1981).
- ³²E. E. Krasovskii, Phys. Rev. B **56**, 12 866 (1997).
- ³³E. E. Krasovskii and W. Schattke, Phys. Rev. B **56**, 12 874 (1997).
- ³⁴E. E. Krasovskii and W. Schattke, Phys. Rev. B **63**, 235112 (2001).
- ³⁵Alternatively, the boundary conditions of an isolated slab may be imposed, see, e.g., E. Wimmer, H. Krakauer, M. Weinert, and A. J. Freeman, Phys. Rev. B **24**, 864 (1981).
- ³⁶To calculate integrals similar to those of Eq. (10) out of an APW representation, Stiles and Hamann (Ref. 26) expanded the step function of cut muffin-tins in an angular momentum series, and Wachutka (Ref. 24) and Hummel and Bross (Ref. 25) simply reduced the muffin-tin radii in order to be able to use the plane-wave representation of the wave functions outside the muffin-tins. To introduce the boundary values, Stiles and Hamann (Ref. 26) generated the values on a real space mesh and then used an FFT procedure to get a 2D reciprocal lattice expansion. An alternative technique was used by Ishida (Ref. 27) who introduced a buffer region between a curvy matching surface and an artificial planar surface and defined the boundary conditions on the planar surface by integrating the Schrödinger equation in the buffer region.
- ³⁷The application of the local γ transformation to the representation of the crystal density in self-consistent calculations has been introduced in E. E. Krasovskii, F. Starrost, and W. Schattke, Phys. Rev. B **59**, 10 504 (1999) and to the calculation of the dielectric matrix in E. E. Krasovskii and W. Schattke, *ibid.* **60**, R16 251 (1999).
- ³⁸E. E. Krasovskii and W. Schattke, Phys. Rev. B **59**, R15 609 (1999).
- ³⁹R. C. Jaklevic and L. C. Davis, Phys. Rev. B **26**, 5391 (1982).
- ⁴⁰V. N. Strocov, R. Claessen, G. Nicolay, S. Hüfner, A. Kimura, A. Harasawa, S. Shin, A. Kakizaki, H. I. Starnberg, P. O. Nilsson, and P. Blaha, Phys. Rev. B **63**, 205108 (2001).
- ⁴¹E. E. Krasovskii, W. Schattke, V. N. Strocov, and R. Claessen, Phys. Rev. B **66**, 235403 (2002).
- ⁴²E. V. Chulkov, V. M. Silkin, and P. M. Echenique, Surf. Sci. **437**, 330 (1999).
- ⁴³E. E. Krasovskii and W. Schattke, Phys. Rev. Lett. **93**, 027601 (2004).
- ⁴⁴D. D. Koelling and B. N. Harmon, J. Phys. C **10**, 3107 (1977).